Geophysical Research Letters

RESEARCH LETTER
10.1029/2023GL104539

Soil Moisture Dominates the Forest Productivity Decline During the 2022 China Compound Drought-Heatwave Event

Dayang Zhao[1,2], **Zhaoying Zhang**[1,2], **and Yongguang Zhang**[1,2,3]

[1]Jiangsu Center for Collaborative Innovation in Geographical Information Resource Development and Application, International Institute for Earth System Sciences, Nanjing University, Nanjing, China, [2]Jiangsu Provincial Key Laboratory of Geographic Information Science and Technology, Key Laboratory for Land Satellite Remote Sensing Applications of Ministry of Natural Resources, School of Geography and Ocean Science, Nanjing University, Nanjing, China, [3]International Joint Carbon Neutrality Laboratory, Nanjing University, Nanjing, China

Key Points:

- Soil moisture (SM), rather than vapor pressure deficit, dominates the forest productivity decline in the 2022 China compound drought-heatwave event
- Forest productivity would decline sharply once SM drops below a certain threshold during extreme compound drought-heatwave events
- Evolution of the 2022 China compound drought-heatwave event and its impacts on forests were illuminated

Supporting Information:

Supporting Information may be found in the online version of this article.

Correspondence to:

Y. Zhang,
yongguang_zhang@nju.edu.cn

Citation:

Zhao, D., Zhang, Z., & Zhang, Y. (2023). Soil moisture dominates the forest productivity decline during the 2022 China compound drought-heatwave event. *Geophysical Research Letters*, *50*, e2023GL104539. https://doi.org/10.1029/2023GL104539

Received 17 MAY 2023
Accepted 23 AUG 2023

Author Contributions:

Conceptualization: Dayang Zhao, Zhaoying Zhang, Yongguang Zhang
Formal analysis: Dayang Zhao, Zhaoying Zhang
Funding acquisition: Yongguang Zhang
Investigation: Dayang Zhao, Zhaoying Zhang
Methodology: Dayang Zhao, Zhaoying Zhang
Project Administration: Yongguang Zhang
Supervision: Yongguang Zhang
Visualization: Dayang Zhao

Abstract Compound drought-heatwave (CDHW) events threaten ecosystem productivity and are often characterized by low soil moisture (SM) and high vapor pressure deficit (VPD). However, the relative roles of SM and VPD in constraining forest productivity during CDHWs remain controversial. In the summer of 2022, China experienced a record-breaking CDHW event (DH2022). Here, we applied satellite remote-sensing data and meteorological data, and machine-learning techniques to quantify the individual contributions of SM and VPD to forest productivity variations and investigate their interactions during the development of DH2022. The results reveal that SM, rather than VPD, dominates the forest productivity decline during DH2022. We identified a possible critical tipping point of SM below which forest productivity would quickly decline with the decreasing SM. Furthermore, we illuminated the evolution of SM, VPD, evapotranspiration, forest productivity, and their interactions throughout DH2022. Our findings broaden the understanding of forest response to extreme CDHWs at the ecosystem scale.

Plain Language Summary Low soil moisture (SM) and high vapor pressure deficit (VPD) are widely recognized as the dominant drivers of forest productivity decline during compound drought-heatwave (CDHW) events. In the summer of 2022, a record-breaking CDHW (DH2022) struck China. In this study, we decoupled the respective impacts of SM and VPD in determining forest productivity decline during DH2022. We found that during DH2022, SM, rather than VPD, is the dominant driver of forest productivity decline, and once SM decreases below a certain threshold, forest productivity would decline sharply. We illuminated the evolution of SM, VPD, evapotranspiration, forest productivity, and their interactions throughout DH2022. Our findings promote the understanding of forest response to extreme CDHWs at the ecosystem scale and thus potentially improve terrestrial ecosystem models' ability to evaluate and predict the impacts of CDHWs.

1. Introduction

Compound drought-heatwave (CDHW) events represent one of the most severe climatic hazards to both natural and human systems. Low soil moisture (SM) supply and high atmospheric vapor demand (driven by vapor pressure deficit, VPD) are widely recognized as the dominant factors driving forest productivity variations during CDHWs (Allen et al., 2010; Salomón et al., 2022). SM represents a direct water pool that determines how much water plant roots can extract. Subseasonal and interannual SM variations can influence short- and long-term ecosystem productivity (Green et al., 2019; Liu et al., 2020). High VPD caused by elevated temperature and soil-atmosphere feedback (Zhou et al., 2019) may induce plants to close leaf stomata to minimize water loss and further reduce plant photosynthesis (Oren et al., 1999). Accurately evaluating the sensitivity of forest productivity to SM and VPD during CDHWs is critical to effectively mitigate the drought-related risks and reduce uncertainties of terrestrial ecosystem models in quantifying the impacts of dryness stress on forests.

However, since SM and VPD are strongly coupled due to land-atmosphere feedback, particularly in CDHWs (Liu et al., 2020; Zhou et al., 2019), the relative importance of SM and VPD in determining ecosystem productivity is still under debate. Previous studies have emphasized the importance of VPD in regulating ecosystem water and carbon flux (Novick et al., 2016; Sulman et al., 2016). Recently, there is also evidence that SM dominates dryness stress on ecosystem productivity compared to VPD (Liu et al., 2020). Besides, few studies pay attention to the development of CDHWs when considering the impacts of SM and VPD. Consequently, discrepancies in

Writing – original draft: Dayang Zhao, Zhaoying Zhang
Writing – review & editing: Dayang Zhao, Zhaoying Zhang, Yongguang Zhang

simulating water stress on ecosystems contribute to large uncertainties for terrestrial ecosystem models or satellite models in evaluating and forecasting the impacts of CDHWs on forests (Knorr & Heimann, 2001; Stocker et al., 2019).

In the summer of 2022, China experienced an extreme CDHW event (hereafter referred to as DH2022). The average national temperature was up to 1.1°C higher than the long-term means, the highest recorded during the same period since 1961 (NCC-CMA, 2022). In some areas, the daily maximum temperature exceeded 42°C. National precipitation deficits were up to 40.9 mm, 12.3% below the average, and 20%–50% across several regions (NCC-CMA, 2022). DH2022 threatened the national electric grid and water safety, cascaded into other hazards including wildfires and crop yield losses, and caused numerous heat-related deaths. Yet, DH2022 also provides an opportunity to assess the relative importance of low SM and high VPD in extreme CDHWs.

Here, we applied satellite remote-sensing and meteorological data to quantify the individual contributions of SM and VPD to forest productivity variations during DH2022 using a machine-learning method. We aim to disentangle the relative roles of SM and VPD in determining forest productivity and further investigate their interactions along with the development of DH2022. The results can advance the understanding of forest response to extreme CDHWs and therefore potentially improve terrestrial ecosystem models for better assessment and prediction of CDHW impacts.

2. Data and Methods

2.1. Study Area

This study focused on the southern region of China (<□33°N), which was the most severely-affected area during DH2022. The ecosystem is representative of evergreen broadleaf forests covering large areas in southern China (Figure S1 in Supporting Information S1), and areas dominated by evergreen broadleaf forests were selected to reduce the differences in vegetation types. To further investigate the specific response of forests to DH2022 development and reduce spatial heterogeneity, we selected 3 areas of interest with a size of 1.25° longitude × 1° latitude: AOI_{l1}, AOI_{l2}, and AOI_s. In addition to suffering from the severe CDHW in July and August (temperature anomaly ≥1.5°C, precipitation anomaly ≤−40%), the three AOIs are characterized by distinctive gross primary productivity (GPP) temporal variations (Table S1 in Supporting Information S1) representing the typical patterns of GPP variations in the study area.

2.2. Data Collection

The meteorological data used in this study, including precipitation (P), 2m air temperature (T2m), potential evapotranspiration (PET), evapotranspiration (ET), soil volumetric water in the layer of 0–7 cm, 7–28 cm, and 28–300 cm (SM_1, SM_2, SM_3), photosynthetically active radiation (PAR) and VPD, were obtained or derived from an enhanced global data set for the land component of the fifth generation of European ReAnalysis (ERA5-Land) from 1992 to 2022 with a spatial resolution of 0.1° × 0.1°(Muñoz-Sabater et al., 2021).

The Moderate Resolution Imaging Spectroradiometer (MODIS) enhanced vegetation index (EVI) (Didan, 2021), TROPOspheric Monitoring Instrument (TROPOMI) solar-induced chlorophyll fluorescence (SIF) (Köhler et al., 2018), and FluxSat GPP (Joiner & Yoshida, 2020) were used to evaluate vegetation dynamics during DH2022. However, there were available observations of only 3 days in August 2022, and SIF analysis thus excluded August 2022. To distinguish the vegetation types in the study area, the MODIS Land Cover Type (MCD12Q1) Version 6.1 data product (Friedl & Sulla-Menashe, 2022) in 2021 was applied (Figure S1 in Supporting Information S1). The specific data introduction and processing were presented in Text S1 in Supporting Information S1. SM data set from ERA5-Land was also compared with that from SMCI1.0 (SM of China by in situ data, version 1.0) based on in situ measurement and machine learning (Q. Li et al., 2022) to assess its reliability (Text S2 and Figure S2 in Supporting Information S1).

2.3. Anomaly Calculation

For the comparability between different variables, we calculate anomalies of climatic factors and vegetation dynamics (ΔVar) as:

$$\Delta Var = \frac{Var - \overline{Var}}{\overline{Var}} \quad (1)$$

where Var is the 2022 value of variables including P, PAR, VPD, $SM_{1\text{-}3}$, EVI, SIF, and GPP, and $\overline{\text{Var}}$ is the average value for 2018–2021. As trends may exist in the long-term time series due to climatic or anthropogenic factors such as CO_2 fertilization (Mohammed et al., 2022; Páscoa et al., 2020), the averages of 2018–2021 were selected as a benchmark. In terms of T2m, the anomaly ΔT2m was defined as the difference between the 2022 value and the 2018–2021 average value to prevent excessively low values.

2.4. Decoupling the Relative Roles of SM and VPD

2.4.1. Calculating the Individual Contributions of Climatic Factors

eXtreme Gradient Boosting (XGBoost) is a widely used machine learning algorithm used for supervised regression and classification problems based on the gradient boosting framework (Chen & Guestrin, 2016). The training about the XGBoost model was presented in Text S3 in Supporting Information S1. In the selected AOIs, the contributions of each climatic factor including $SM_{1\text{-}3}$, T2m, P, PAR, VPD, and EVI, were calculated the following three steps: (a) for each trained model, the unmodified predictors were input to get the prediction $Pred_0$. Then, the predictors where the 2022 value of the target variable was replaced with the 2018–2021 average were input to get the prediction $Pred_{var}$; (b) the difference S_{var} between $Pred_0$ and $Pred_{var}$ was calculated for each model; (c) the average and standard deviation of S_{var} from all models were calculated as the contribution of each climatic factors and the error, respectively. The caveats in using the XGBoost algorithm for attributions were also discussed in Text S5 in Supporting Information S1.

2.4.2. Regional Analysis

For the entire study area, the GPP anomaly (ΔGPP) across all pixels from July to October was divided into high level (≤−15%) and low level (>−15%), and then the distributions of ET, SM, VPD, and SIF anomaly (ΔSIF) were analyzed for each level. The selection of the threshold and its impacts on conclusions were discussed in Text S6 in Supporting Information S1. Moreover, to investigate the correlation among SM, VPD, and GPP, we sorted the VPD and SM into 10 × 10 percentile bins and calculated the mean ΔGPP and ΔSIF of each percentile bin across all pixels from July to October. It should be noted that since SM_2 was strongly correlated with SM_1 and SM_3 (Figure S3 in Supporting Information S1), and contributed most to ΔGPP and ΔSIF (See Results 3.2), SM_2 was selected to represent SM variations.

3. Results

3.1. Climate and Vegetation Variations During DH2022

We analyzed the spatiotemporal variations of climatic factors during DH2022. In July and August, high positive ΔT2m, positive ΔPAR, and negative Δ*P* were widespread in China, particularly in southern China, where local extremes of T2m and P (ΔT2m > 2°C, Δ*P* < −50%) occurred (Figure S4 in Supporting Information S1). Moreover, relative to severe and moderate drought, extreme drought accounted for the largest proportion (>47%) of all drought-affected areas (Figure S5 in Supporting Information S1). Compared to the past 30 years, the extent of drought and the proportion of extreme drought were the highest during the same period (Figure S5 in Support-ing Information S1). Simultaneously, high negative ΔSM (<−30%) in southern China started in July, peaked in August and September, and receded in October (Figure 1a). High positive ΔVPD (>80%) developed similarly to ΔSM from August to October but appeared in many parts of southern China in July (Figure 1b).

ΔSIF and ΔGPP captured the forest productivity variations. As shown in Figures 1c and 1d. The spatial distributions of ΔSIF and ΔGPP were consistent but the magnitude of ΔSIF was higher than that of ΔGPP, possibly because the small variations in SIF caused the large variations in anomalies (as the denominator was a small value) due to the weak signal of SIF. In southern China dominated by evergreen broadleaf forests, SIF, and GPP were nearly normal or even increased (ΔGPP: −10%–+10%, ΔSIF: −30%–30%) in July and generally declined (ΔGPP: −10% – 0, and <−25% in some areas, ΔSIF was missing) in August. In September and October, the extent of high negative ΔSIF (<−30%) and ΔGPP (<−20%) continued expanding. Notably, in some areas such as southeast coasts subjected to severe drought and heatwave in July and August, SIF and GPP remained near-normal from July to October. ΔEVI, capturing forest structure variations, also exhibited a relatively consistent spatiotemporal pattern with ΔSIF and ΔGPP (Figure S6 in Supporting Information S1). The results revealed that there seem to be 3 typical patterns of forest GPP variations during DH2022: (a) a substantial decline in

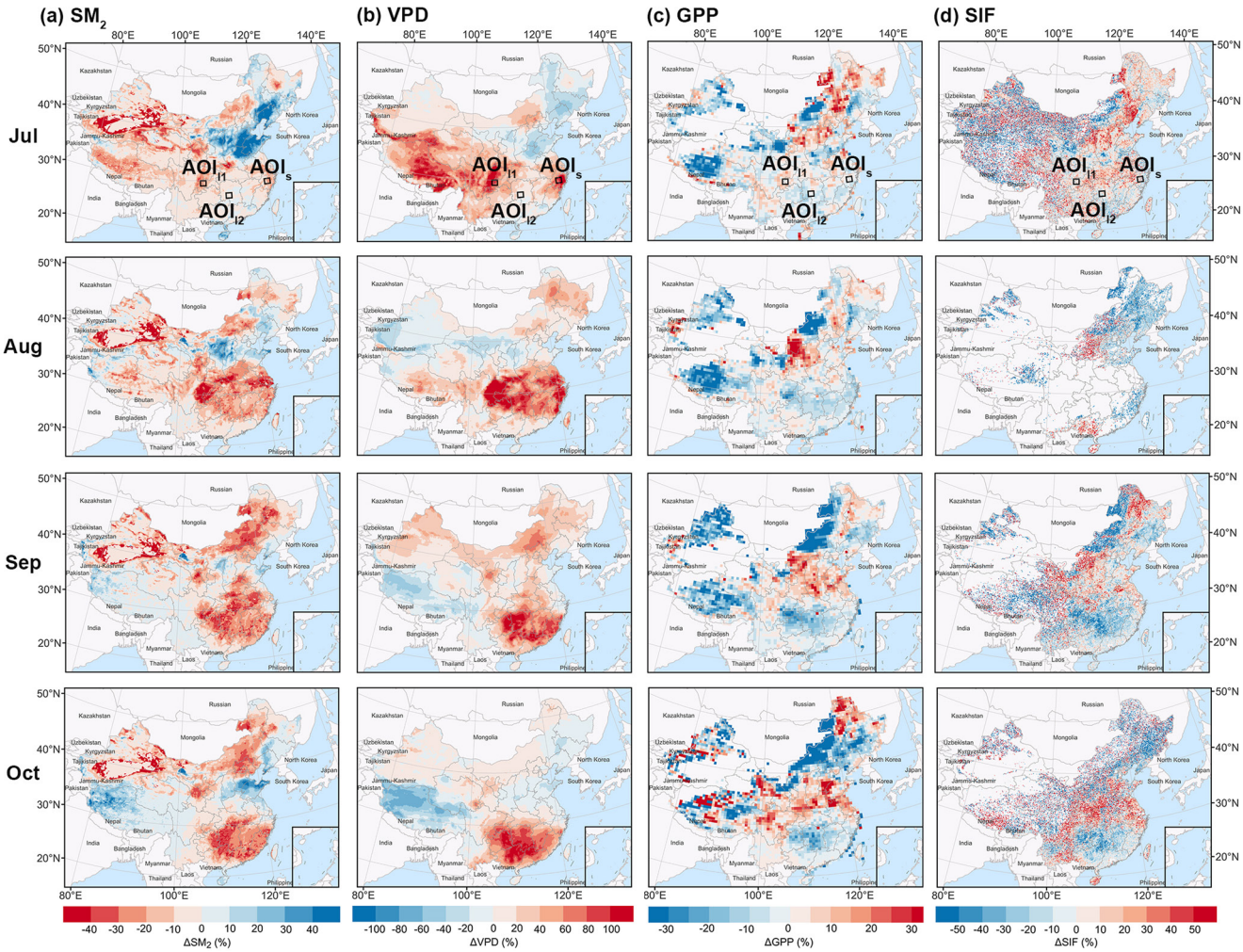

Figure 1. Climate and vegetation variations from July to October: (a) Soil Moisture in the layer of 7–28 cm (SM_2); (b) vapor pressure deficit; (c) gross primary productivity; (d) solar-induced chlorophyll fluorescence (SIF). SIF data for August 2022 was missing. The square denotes the selected areas of interest.

August when DH2022 was the most severe, followed by a recovery in subsequent months (e.g., AOI_{I1}); (b) an intensifying decline from July to September or October when the heatwave receded (e.g., AOI_{I2}); (c) near-normal variations from July to October (e.g., AOI_S).

3.2. Contributions of SM and VPD to Forest Productivity Variations During DH2022

The XGBoost algorithm demonstrates high performance in predicting ΔGPP with a mean absolute error of 1.66% and acceptable performance in predicting ΔSIF with a mean absolute error of 12.78% (Figure S7 in Supporting Information S1). The trained models were then used to compare the contributions of SM and VPD with other climatic factors during DH2022 in three AOIs with typical patterns of GPP variations. As presented in Figure 2, in general, SM_2 and VPD were dominant factors affecting ΔGPP and ΔSIF from July to October in all AOIs, with SM_2 contributing more than VPD when ΔGPP and ΔSIF were lower than −15% and −30%, respectively. However, the impacts of EVI on ΔGPP and ΔSIF were not evident.

AOI_{I1} was the most affected area by DH2022 in July and August (Figures 2a and 2b). However, despite significant decreases in SM and increases in VPD compared to their levels of the same period in 2018–2021 (hereafter referred to as the historical level) in July, GPP and SIF remained close to the historical level. In August, when VPD and SM_2 reached their highest (□2.9 kPa) and lowest (□0.17 m^3/m^3) levels, respectively, ΔGPP exceeds −25% with VPD and SM_2 contributing similarly and most (□12%/26%). In September, VPD was nearly normal,

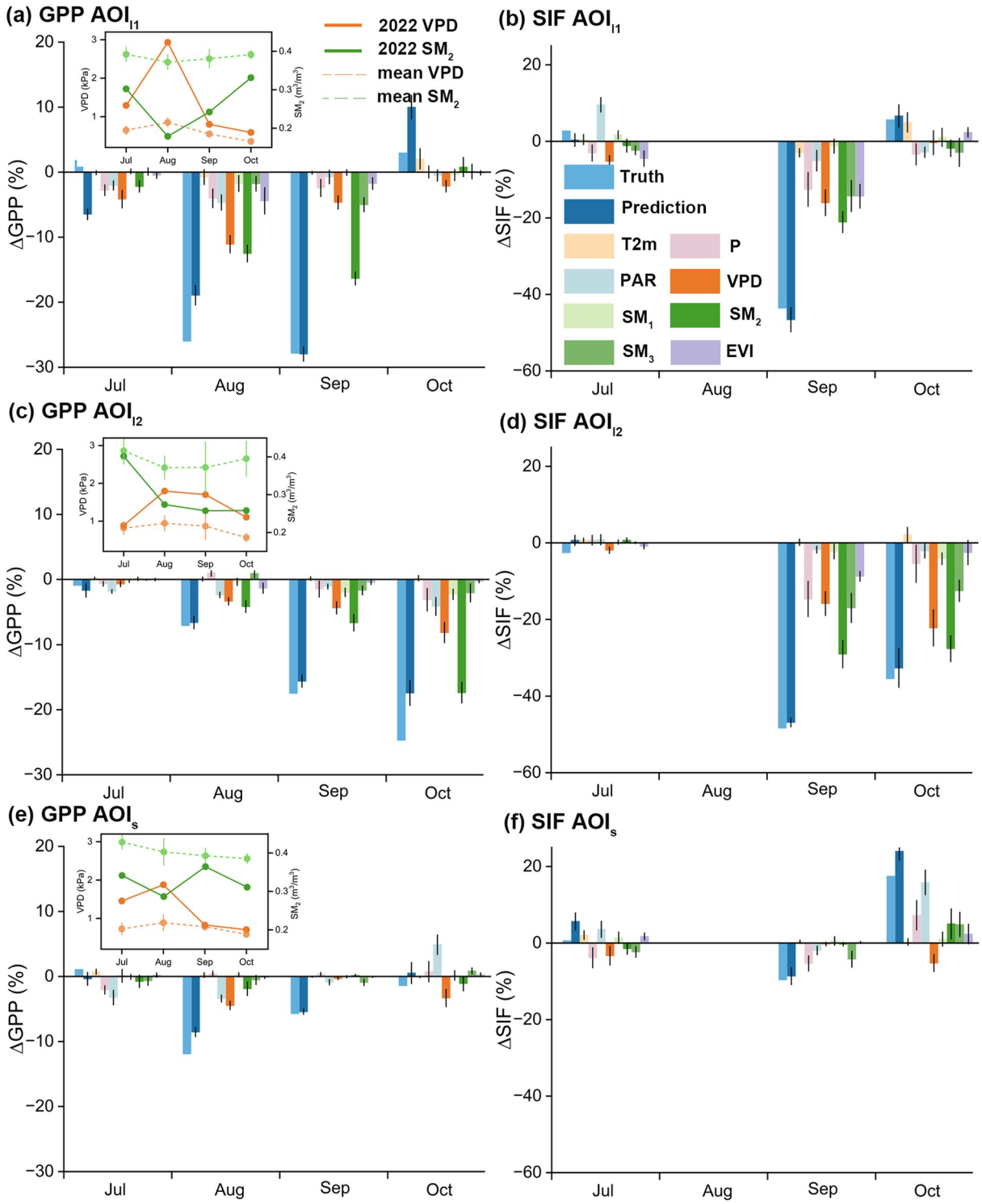

Figure 2. Contributions of various climatic factors to ΔGPP and ΔSIF in the selected AOIs: (a) gross primary productivity (GPP) AOI$_{l1}$, (b) SIF AOI$_{l1}$, (c) GPP AOI$_{l2}$, (d) SIF AOI$_{l2}$, (e) GPP AOI$_s$, (f) GPP AOI$_s$. The upper right panels in the GPP plots are the dynamics of SM$_2$ and vapor pressure deficit in the corresponding AOIs from July to October. The legends Truth and Prediction denote the FluxSat-derived (TROPOMI-derived) and model-predicted ΔGPP (ΔSIF), respectively.

and SM_2 increased slightly but remained at an extremely low level (□0.24 m^3/m^3). ΔGPP and ΔSIF fell to −27.8% and −43.6%, respectively, with SM_2 the dominant factor (ΔGPP: □17.9%/27.8%, ΔSIF: □21.08%/43.6%). The difference between August and September implies that a large productivity decline did not necessarily occur with high VPD.

AOI_{l2} exhibited high negative ΔGPP and ΔSIF in September and October (Figures 2c and 2d). In August, VPD peaked (□1.8 kPa), SM_2 decreased from 0.40 m^3/m_3 to 0.27 m^3/m^3, and GPP declined by □7% relative to the historical level. In September and October, VPD was down slightly but still close to double the historical level, and SM_2 continued decreasing slightly. Conversely, GPP and SIF declined sharply relative to the historical level. It appears that a slight SM_2 decrease around a certain value induced the sharp forest productivity decline.

Compared with AOI_{l1} and AOI_{l2}, AOI_s was mildly influenced by DH2022 (Figures 2e and 2f), with GPP remaining close to the historical level from July to October except for August. Although SM_2 varied from July to October, its contribution to forest ΔGPP and ΔSIF was not evident, suggesting SM_2 within a certain range may be not a limitation for AOI_s during DH2022.

3.3. Relative Roles of VPD and SM During DH2022

The data across the entire study area from July to October were aggregated to disentangle the relative roles of VPD and SM in determining forest productivity during DH2022 (Figure 3). As shown in Figure 3a, b, a threshold (40th percentile, □0.34 m^3/m^3) appeared to exist in the response of forest GPP and SIF to SM_2. When SM_2 fell below this threshold, its negative impact on forest GPP and SIF became significantly more intense (ΔGPP<−10%; ΔSIF<−15%). The threshold for SM_2 could also be found in the high-level (<−15%) ΔGPP from August to October, except for July when the water stress may not be the dominant limitation (Figure 3c). However, a range of ΔGPP and ΔSIF values from low (>−5%) to high (<−10%) could be observed across all VPD percentiles, and despite VPD exceeding the extremely high level, low ΔGPP and ΔSIF (>−5%) could exist (Figures 3a and 3b). ΔSIF exhibited a consistent pattern with ΔGPP in September and October (Figure 3c). The difference in VPD between high-level (<−15%) and low-level (>−15%) ΔGPP was not significant (<0.2 kPa) in September and October (Figure 3c). Overall, during DH2022, substantial forest GPP and SIF decline generally occurred with extremely low SM but not necessarily with high VPD. The threshold response of forest productivity may exist in SM rather than VPD. Furthermore, the difference in ΔEVI between high-level and low-level ΔGPP was not remarkable. In July, the ΔEVI of high-level ΔGPP was even positive and higher than that of low-level ΔGPP (Figure S8a in Supporting Information S1). These findings suggested that the dynamics of GPP and EVI may be not synchronized.

ET as the bridge of land-atmosphere water and energy exchange was selected to analyze the interactions between SM and VPD during DH2022. ET was higher in July, but gradually lower from August to October, than the historical level (Figure S8b in Supporting Information S1), implying DH2022 significantly altered the land-atmosphere flux. Figure 3d displayed the relationships among SM_2, VPD, and ET. SM_2 decreased rapidly when VPD was in the range of 0–1.5 kPa, while the rate of decrease slowed down when VPD exceeded 1.5 kPa. High VPD (>2 kPa) tended to be accompanied by low SM_2 (<0.3 m^3/m^3). High ET (>3 mm/d) occurred at moderate or higher VPD (>□0.8 kPa) but also required adequate SM_2. This pattern could also be observed in SM_1 and SM_3 (Figure S9 in Supporting Information S1). As presented in Figure 3c, in July and August, ET and VPD showed a consistent difference between high-level and low-level ΔGPP. However, in September and October, although the VPD of high-level ΔGPP was slightly higher than that of low-level ΔGPP, the difference between high-level and low-level ΔGPP was consistent for ET and SM_2. It appears that ET was determined by VPD in July and August but by SM in September and October during DH2022.

4. Discussion and Conclusions

The dry-hot extreme that struck China in the summer of 2022 was a record-breaking compound climate hazard but also provided an opportunity to assess the relative importance of low SM and high VPD in extreme CDHWs. This study attempted to disentangle the individual effects of SM and VPD on forest productivity and further investigate their interactions during the development of DH2022.

Our findings revealed that a substantial reduction in GPP and SIF was associated with low SM, but not necessarily high VPD during DH2022. Consistent with a recent global assessment of SM and VPD stress on ecosystem

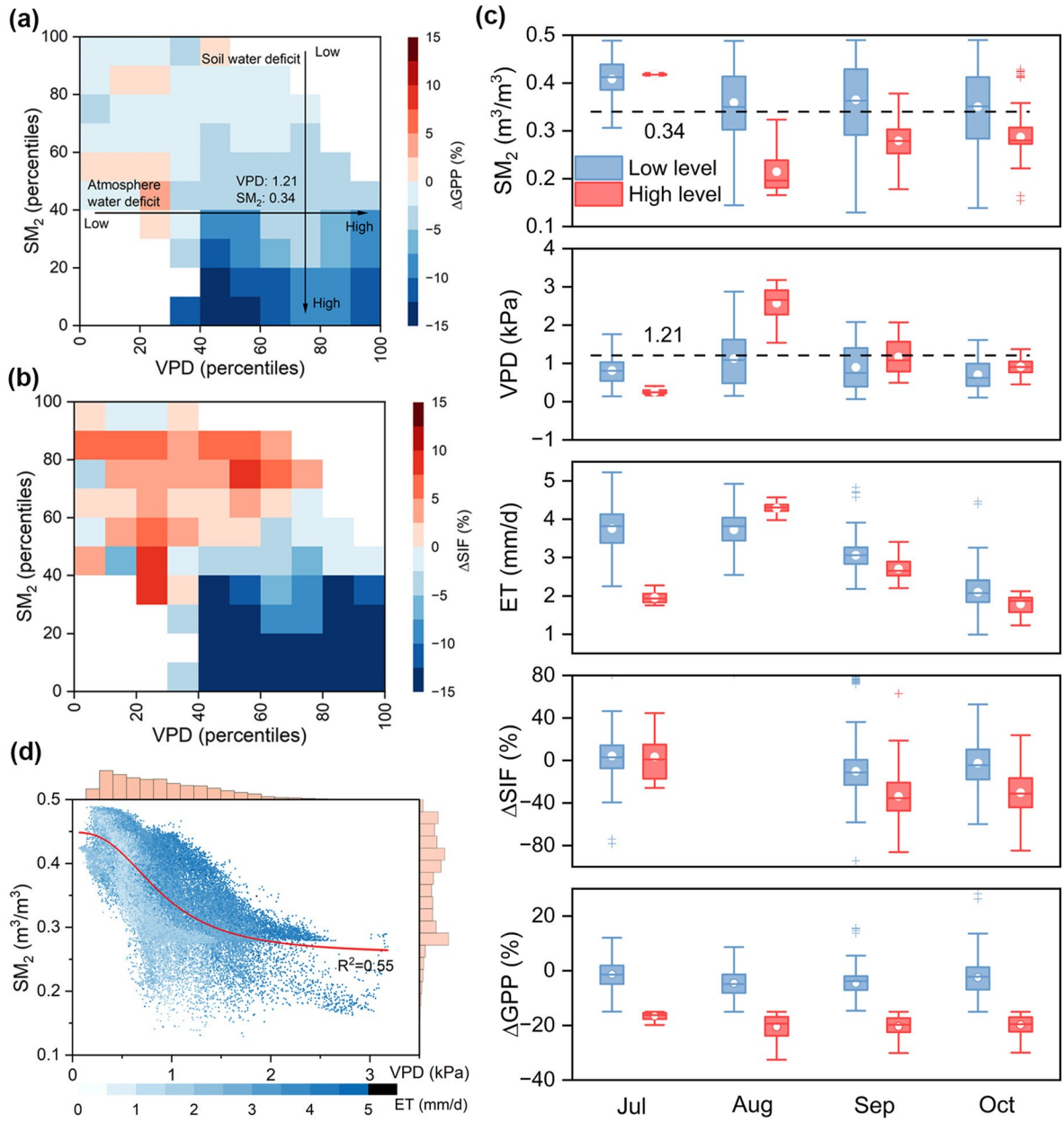

Figure 3. Correlation of vapor pressure deficit (VPD), SM_2, ΔSIF, and ΔGPP from July to October in 2022 across the study area: (a) Mean ΔGPP in each percentile bin of SM_2 and VPD, (b) Mean ΔSIF in each percentile bin of SM_2 and VPD, (c) VPD, SM_2, ET, ΔSIF for high level (<−15%) and low level (>−15%) ΔGPP per month. In the boxplot, the white circles, center lines, cross marks, and box bounds indicate the mean values, median values, extremes, and 25th/75th percentile values, respectively; and the whiskers indicate the 25th/75th percentile values plus or minus 1.5 × (75th percentile values − 25th percentile values). 1.21 kPa and 0.34 m^3/m^3, as the 25 percentiles of VPD and SM_2 in the study area from July to October 2018–2021, respectively, were used as the reference of the extreme level. (d) Scatters of SM_2, VPD, and ET. The color of the scatters represents the magnitude of ET. The histograms on the top and right represent the density of data points along the VPD axis and the SM_2 axis, respectively. The red line is the fit line of VPD and SM_2.

production concluding that SM dominated dryness stress on ecosystem production (Liu et al., 2020), our results further demonstrated that this conclusion still held for forests under extreme CDHWs. VPD could indeed reduce stomatal closure, leading to a decline in GPP (Figure 2). However, when SM was sufficient, plant root systems can effectively absorb water, allowing photosynthesis to occur even with the partial stomatal closure induced by high VPD. Moreover, the plants can actively regulate stomatal conductance to improve the water-use efficiency (the gain of carbon per unit of water loss) in response to high VPD (Bastos et al., 2020; Peters et al., 2018). Consequently, the sensitivity of forest productivity to VPD may be moderate when SM is sufficient during CDHWs.

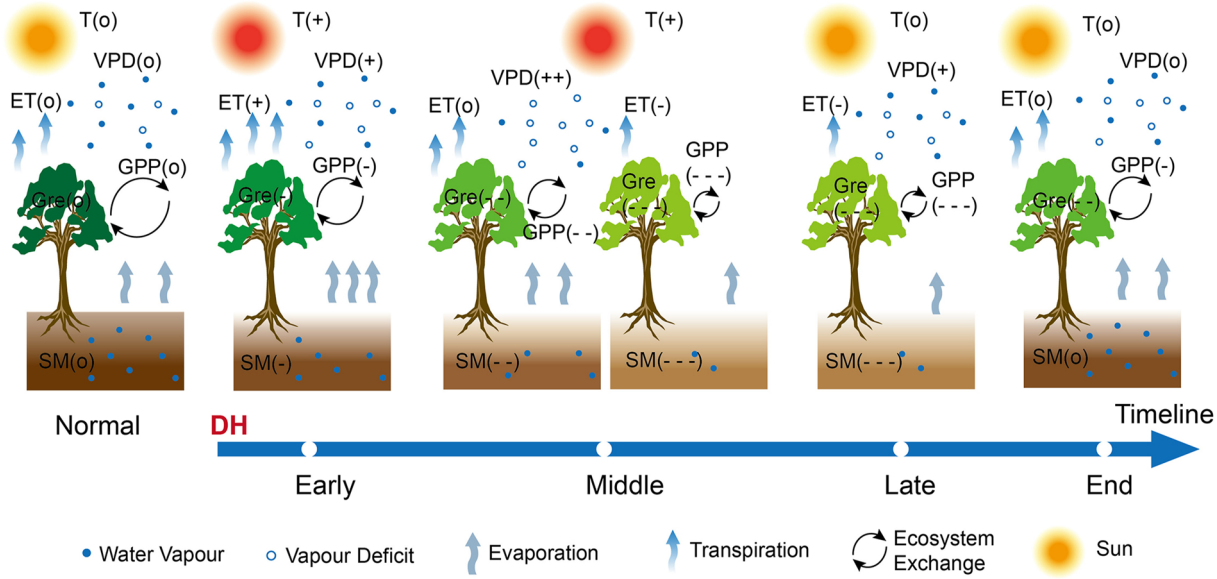

Figure 4. Schematic diagram of DH2022 impacts on forest productivity. T, vapor pressure deficit (VPD), ET, gross primary productivity (GPP), Gre, and soil moisture (SM) indicate temperature, VPD, evapotranspiration, GPP, greenness, and SM, respectively. Symbols (o), (+), and (−) denote normal, increase, and decrease, respectively, relative to the historical period. The amount of symbols indicates the magnitude (e.g., (++) indicates severely higher than the historical level, and (---) indicates extremely lower than the historical level). It is noted that the normal stage refers to the normal conditions in the same period, and the comparison between each stage and the normal stage should be in the same period.

In contrast, GPP and SIF would decline largely and rapidly once SM dropped below a certain threshold (Figures 2 and 3), which has been demonstrated in tropical rainforests (Meir et al., 2015). Although the root system could penetrate the deep-water zone and resist slight-to-mild SM deficiencies, forests would suffer destruction or even death when SM dropped to a threshold where stomatal closure was further reinforced and the hydraulic transfer from soils to leaves was impaired (Sperry et al., 2002). In our study, the threshold was identified as □0.34 m^3/m_3 in SM_2 (ΔSM_2: □ ⅁30%), which resulted in a reduction of approximately 15% in GPP in southern China during DH2022. A recent study pointed out that such threshold occurred at values > 10th percentile of soil water anomalies in □70% of global areas, suggesting that vegetation can respond sharply even when the drought stress was smaller than the severity of those 1-in10 worst drought events in many locations (X. Li et al., 2023). The thresh-old decreased from low to high forest coverage due to the presence of a deeper root system in denser forests. Additionally, forests in tropical climates exhibited a much higher threshold (i.e., lower resistance) than those in temperate and boreal climates, possibly associated with a higher sensitivity of vegetation in tropical areas to drought stress (X. Li et al., 2023).

However, we found that high VPD tended to occur with extremely low SM (Figure 3), potentially due to ET variations during DH2022. The strong correlation between SM and VPD constituted a confounding factor, which was frequently overlooked when assessing their impacts on forest productivity, particularly during CDHWs (Liu et al., 2020). Elevated temperature can increase atmospheric water demand, and high VPD can exacerbate SM depletion by enhancing ET (Teuling et al., 2013). In turn, the reduction of SM due to the initial precipitation deficit can reduce ET, thereby enhancing the heating and drying of the near-surface atmosphere, leading to higher VPD (Miralles et al., 2014). The decrease in ET further lowered land-atmosphere water exchange, increased sensible heat, and suppressed cloud formation and precipitation, ultimately exacerbating both soil and atmosphere water deficits (Seneviratne et al., 2010). Moreover, this land-atmosphere feedback was projected to be enhanced by climate warming, resulting in stronger correlations between SM and VPD and hence the more frequent occurrence of CDHWs (Dirmeyer et al., 2012; Zhou et al., 2019).

Overall, the impact process of DH2022 on forests can be divided into four stages at a monthly scale (Figure 4): (a) Early phase (i.e., July). Sufficient SM can support enhanced ET to alleviate VPD outbreaks due to elevated temperature. Yet, the increase in VPD reduced GPP (SIF) and hence greenness. (b) Middle phase (i.e., August). High temperature and precipitation deficit persist. The decrease in SM due to precipitation deficit weakened ET, intensifying higher VPD, while higher VPD exacerbated SM depletion. High VPD and low SM continued to

reduce GPP and hence greenness, and once SM decreased below a certain threshold, GPP and greenness declined sharply. (c) Late phase (i.e., September or October). High temperature retreated but precipitation deficit persisted. Extreme low SM resulted in lower ET and thus higher VPD than normal during the same period. GPP and greenness remained at extremely low levels compared with normal conditions. (d) End phase. Precipitation replenished SM, and temperature, SM, VPD, and ET returned to normal. Yet, the recovery of plant growth and ecosys-tem productivity entailed months or even years, which remained controversial (Anderegg et al., 2015; Schwalm et al., 2017). The relationship between greenness and productivity during CDHWs, and the specific evolution of forests and CDHWs were discussed in Text S7 and Text S8 in Supporting Information S1, respectively. Accu-rately understanding the progression of CDHWs provides valuable insights for forest drought management strate-gies. For example, regulating SM (e.g., irrigation) before reaching critical thresholds may effectively alleviate the damage of CDHWs on forest productivity. Land-atmosphere feedback characterized by the interactions between SM, VPD, and ET is needed to be considered when estimating the response of the carbon cycle to climatic change globally, as well as when conducting field-scale investigations of the response of the ecosystem to CDHWs.

This study disentangled the relative roles of VPD and SM in determining forest productivity during the development of this extreme CDHW event in China, and demonstrated that SM, rather than VPD, dominates the forest productivity decline at the monthly scale during extreme CDHWs. We identified a possible critical tipping point of SM below which forest productivity would quickly decline with the decreasing SM. Furthermore, we illuminated the evolution of SM, VPD, evapotranspiration, forest productivity, and their interactions throughout DH2022. These findings broaden the understanding of forest response to CDHWs at the ecosystem scale and thus potentially improve terrestrial ecosystem models' ability to evaluate and predict the impacts of CDHWs.

Data Availability Statement

ERA5-Land data can be downloaded at https://doi.org/10.24381/cds.68d2bb30. FluxSat data can be downloaded at https://avdc.gsfc.nasa.gov/pub/tmp/FluxSat_GPP. MOD13A1 and MCD12Q1 data can be downloaded at https://doi.org/10.5067/MODIS/MOD13A1.061 and https://doi.org/10.5067/MODIS/MCD12Q1.061, respectively. MODIS-related data were processed at the Google Earth Engine platform (https://code.earthengine.google.com, Gorelick et al., 2017). XGBoost (Chen & Guestrin, 2016) code is publicly available on GitHub (https://github.com/dmlc/xgboost).

Acknowledgments
This research was supported by the National Natural Science Foundation of China (42125105, 42071388, 42101320). The meteorological data used in this study was produced by ERA5-Land and shared by Climate Data Store. We extend our gratitude to the science team directed by Joanna Joiner for producing and sharing FluxSat data sets. Our gratitude also extends to Philipp Koehler and Christian Frankenberg's group for providing the TROPOMI SIF data. We also express our sincere appreciation to the science team members who produced and managed the remote sensing products employed in this study. Lastly, we would like to acknowledge the anonymous reviewers for their insightful and constructive comments, which aided in improving the quality of our manuscript.

References

Allen, C. D., Macalady, A. K., Chenchouni, H., Bachelet, D., McDowell, N., Vennetier, M., et al. (2010). A global overview of drought and heat-induced tree mortality reveals emerging climate change risks for forests. *Forest Ecology and Management*, *259*(4), 660–684. https://doi.org/10.1016/j.foreco.2009.09.001

Anderegg, W. R., Schwalm, C., Biondi, F., Camarero, J. J., Koch, G., Litvak, M., et al. (2015). Pervasive drought legacies in forest ecosystems and their implications for carbon cycle models. *Science*, *349*(6247), 528–532. https://doi.org/10.1126/science.aab1833

Bastos, A., Ciais, P., Friedlingstein, P., Sitch, S., Pongratz, J., Fan, L., et al. (2020). Direct and seasonal legacy effects of the 2018 heat wave and drought on European ecosystem productivity. *Science Advances*, *6*(24), eaba2724. https://doi.org/10.1126/sciadv.aba2724

Chen, T., & Guestrin, C. (2016). Xgboost: A scalable tree boosting system. In *Paper presented at the proceedings of the 22nd ACM SIGKDD international conference on knowledge discovery and data mining*.

Didan, K. (2021). MODIS/Terra vegetation indices 16-day L3 global 500m SIN grid V061. In *NASA EOSDIS land processes DAAC*.

Dirmeyer, P. A., Cash, B. A., Kinter, J. L., III., Stan, C., Jung, T., Marx, L., et al. (2012). Evidence for enhanced land–atmosphere feedback in a warming climate. *Journal of Hydrometeorology*, *13*(3), 981–995. https://doi.org/10.1175/jhm-d-11-0104.1

Friedl, M., & Sulla-Menashe, D. (2022). MODIS/Terra+Aqua land cover type yearly L3 global 500m SIN grid V061. In *NASA EOSDIS land processes DAAC*.

Gorelick, N., Hancher, M., Dixon, M., Ilyushchenko, S., Thau, D., & Moore, R. (2017). Google Earth engine: Planetary-scale geospatial analysis for everyone. *Remote Sensing of Environment*, *202*, 18–27. https://doi.org/10.1016/j.rse.2017.06.031

Green, J. K., Seneviratne, S. I., Berg, A. M., Findell, K. L., Hagemann, S., Lawrence, D. M., & Gentine, P. (2019). Large influence of soil moisture on long-term terrestrial carbon uptake. *Nature*, *565*(7740), 476–479. https://doi.org/10.1038/s41586-018-0848-x

Joiner, J., & Yoshida, Y. (2020). Satellite-based reflectances capture large fraction of variability in global gross primary production (GPP) at weekly time scales. *Agricultural and Forest Meteorology*, *291*, 108092. https://doi.org/10.1016/j.agrformet.2020.108092

Knorr, W., & Heimann, M. (2001). Uncertainties in global terrestrial biosphere modeling, Part II: Global constraints for a process-based vegetation model. *Global Biogeochemical Cycles*, *15*(1), 227–246. https://doi.org/10.1029/1998gb001060

Köhler, P., Frankenberg, C., Magney, T. S., Guanter, L., Joiner, J., & Landgraf, J. (2018). Global retrievals of solar-induced chlorophyll fluorescence with TROPOMI: First results and intersensor comparison to OCO-2. *Geophysical Research Letters*, *45*(19), 10456–410463. https://doi.org/10.1029/2018gl079031

Li, Q., Shi, G., Shangguan, W., Nourani, V., Li, J., Li, L., et al. (2022). A 1 km daily soil moisture data set over China using in situ measurement and machine learning. *Earth System Science Data*, *14*(12), 5267–5286. https://doi.org/10.5194/essd-14-5267-2022

Li, X., Piao, S., Huntingford, C., Peñuelas, J., Yang, H., Xu, H., et al. (2023). Global variations in critical drought thresholds that impact vegetation. *National Science Review*, *10*(5), nwad049. https://doi.org/10.1093/nsr/nwad049

Liu, L., Gudmundsson, L., Hauser, M., Qin, D., Li, S., & Seneviratne, S. I. (2020). Soil moisture dominates dryness stress on ecosystem production globally. *Nature Communications*, *11*(1), 4892. https://doi.org/10.1038/s41467-020-18631-1

Meir, P., Wood, T. E., Galbraith, D. R., Brando, P. M., Da Costa, A. C., Rowland, L., & Ferreira, L. V. (2015). Threshold responses to soil moisture deficit by trees and soil in tropical rain forests: Insights from field experiments. *BioScience*, *65*(9), 882–892. https://doi.org/10.1093/biosci/biv107

Miralles, D. G., Teuling, A. J., Van Heerwaarden, C. C., & Vilà-Guerau de Arellano, J. (2014). Mega-heatwave temperatures due to combined soil desiccation and atmospheric heat accumulation. *Nature Geoscience*, *7*(5), 345–349. https://doi.org/10.1038/ngeo2141

Mohammed, S., Alsafadi, K., Enaruvbe, G. O., Bashir, B., Elbeltagi, A., Széles, A., et al. (2022). Assessing the impacts of agricultural drought (SPI/SPEI) on maize and wheat yields across Hungary. *Scientific Reports*, *12*(1), 8838. https://doi.org/10.1038/s41598-022-12799-w

Muñoz-Sabater, J., Dutra, E., Agustí-Panareda, A., Albergel, C., Arduini, G., Balsamo, G., et al. (2021). ERA5-Land: A state-of-the-art global reanalysis data set for land applications. *Earth System Science Data*, *13*(9), 4349–4383. https://doi.org/10.5194/essd-13-4349-2021

NCC-CMA. (2022). October 2022 press conference of China meteorological administration. Retrieved from http://cmdp.ncc-cma.net/cn/monitoring.htm

Novick, K. A., Ficklin, D. L., Stoy, P. C., Williams, C. A., Bohrer, G., Oishi, A. C., et al. (2016). The increasing importance of atmospheric demand for ecosystem water and carbon fluxes. *Nature Climate Change*, *6*(11), 1023–1027. https://doi.org/10.1038/nclimate3114

Oren, R., Sperry, J., Katul, G., Pataki, D., Ewers, B., Phillips, N., & Schäfer, K. (1999). Survey and synthesis of intra-and interspe-cific variation in stomatal sensitivity to vapour pressure deficit. *Plant, Cell and Environment*, *22*(12), 1515–1526. https://doi.org/10.1046/j.1365-3040.1999.00513.x

Páscoa, P., Gouveia, C. M., Russo, A. C., Bojariu, R., Vicente-Serrano, S. M., & Trigo, R. M. (2020). Drought impacts on vegetation in south-eastern Europe. *Remote Sensing*, *12*(13), 2156. https://doi.org/10.3390/rs12132156

Peters, W., van der Velde, I. R., Van Schaik, E., Miller, J. B., Ciais, P., Duarte, H. F., et al. (2018). Increased water-use efficiency and reduced CO_2 uptake by plants during droughts at a continental scale. *Nature Geoscience*, *11*(10), 744–748. https://doi.org/10.1038/s41561-018-0212-7

Salomón, R. L., Peters, R. L., Zweifel, R., Sass-Klaassen, U. G., Stegehuis, A. I., Smiljanic, M., et al. (2022). The 2018 European heatwave led to stem dehydration but not to consistent growth reductions in forests. *Nature Communications*, *13*(1), 28. https://doi.org/10.1038/s41467-021-27579-9

Schwalm, C. R., Anderegg, W. R., Michalak, A. M., Fisher, J. B., Biondi, F., Koch, G., et al. (2017). Global patterns of drought recovery. *Nature*, *548*(7666), 202–205. https://doi.org/10.1038/nature23021

Seneviratne, S. I., Corti, T., Davin, E. L., Hirschi, M., Jaeger, E. B., Lehner, I., et al. (2010). Investigating soil moisture–climate interactions in a changing climate: A review. *Earth-Science Reviews*, *99*(3–4), 125–161. https://doi.org/10.1016/j.earscirev.2010.02.004

Sperry, J., Hacke, U., Oren, R., & Comstock, J. (2002). Water deficits and hydraulic limits to leaf water supply. *Plant, Cell and Environment*, *25*(2), 251–263. https://doi.org/10.1046/j.0016-8025.2001.00799.x

Stocker, B. D., Zscheischler, J., Keenan, T. F., Prentice, I. C., Seneviratne, S. I., & Peñuelas, J. (2019). Drought impacts on terrestrial primary production underestimated by satellite monitoring. *Nature Geoscience*, *12*(4), 264–270. https://doi.org/10.1038/s41561-019-0318-6

Sulman, B. N., Roman, D. T., Yi, K., Wang, L., Phillips, R. P., & Novick, K. A. (2016). High atmospheric demand for water can limit forest carbon uptake and transpiration as severely as dry soil. *Geophysical Research Letters*, *43*(18), 9686–9695. https://doi.org/10.1002/2016gl069416

Teuling, A. J., Van Loon, A. F., Seneviratne, S. I., Lehner, I., Aubinet, M., Heinesch, B., et al. (2013). Evapotranspiration amplifies European summer drought. *Geophysical Research Letters*, *40*(10), 2071–2075. https://doi.org/10.1002/grl.50495

Zhou, S., Williams, A. P., Berg, A. M., Cook, B. I., Zhang, Y., Hagemann, S., et al. (2019). Land–atmosphere feedbacks exacerbate concurrent soil drought and atmospheric aridity. *Proceedings of the National Academy of Sciences of the United States of America*, *116*(38), 18848–18853. https://doi.org/10.1073/pnas.1904955116

References From the Supporting Information

Otkin, J. A., Svoboda, M., Hunt, E. D., Ford, T. W., Anderson, M. C., Hain, C., & Basara, J. B. (2018). Flash droughts: A review and assessment of the challenges imposed by rapid-onset droughts in the United States. *Bulletin of the American Meteorological Society*, *99*(5), 911–919. https://doi.org/10.1175/bams-d-17-0149.1

Wohlfahrt, G., Gerdel, K., Migliavacca, M., Rotenberg, E., Tatarinov, F., Müller, J., et al. (2018). Sun-induced fluorescence and gross primary productivity during a heat wave. *Scientific Reports*, *8*(1), 1–9. https://doi.org/10.1038/s41598-018-32602-z

Wolf, S., Keenan, T. F., Fisher, J. B., Baldocchi, D. D., Desai, A. R., Richardson, A. D., et al. (2016). Warm spring reduced carbon cycle impact of the 2012 US summer drought. *Proceedings of the National Academy of Sciences of the United States of America*, *113*(21), 5880–5885. https://doi.org/10.1073/pnas.1519620113

Yuan, X., Wang, Y., Ji, P., Wu, P., Sheffield, J., & Otkin, J. A. (2023). A global transition to flash droughts under climate change. *Science*, *380*(6641), 187–191. https://doi.org/10.1126/science.abn6301